DOI: https://doi.org/10.24425/amm.2025.155488

WANLALAK SANPHIBOON<sup>⊙</sup><sup>1\*</sup>, TAKAAKI YAGI<sup>1</sup>, ABRAR AHMED<sup>1</sup>, VU NGOC HAI<sup>1</sup>, TAIKI TSUCHIYA<sup>2</sup>, SEUNGWON LEE<sup>2</sup>, NORIO NUNOMURA<sup>2</sup>, SATOSHI MURAKAMI<sup>2</sup>, SUSUMU IKENO<sup>3</sup>, KARIN SHIBATA<sup>4</sup>, HIROAKI MATSUI<sup>4</sup>, TOMOO YOSHIDA<sup>4</sup>, KENJI MATSUDA<sup>2</sup>

## STUDY ON THE PRECIPITATION SEQUENCE IN AI-Zn-Mg WITH LOW Zn/Mg AGED AT 200°C

Al-Zn-Mg alloys are known for their high strength-to-weight ratio. This study focuses on the changes in mechanical and microstructural properties in an alloy with a low Zn/Mg ratio. Micro Vickers hardness results showed that the alloy reached peak hardness during optimal aging, then gradually softened, which is typical of over-aging. TEM analysis focusing on the  $<110>_{Al}$  revealed precipitates such as  $\eta$ ,  $\eta'$ , T, and T' phases that evolved as aging progressed. Initially, the precipitates couldn't be observed, and by peak aging, the coexisting of  $\eta$ ,  $\eta'$ , T, and T' phases became dominant, playing a major role in the hardness. As the aging continued, the precipitates grew, while the number density decreased. This study offers insight into how precipitate phases affect the strength and properties of Al-Zn-Mg alloys when exposed to high temperatures.

Keywords: Al-Zn-Mg alloy; Heat treatment; Precipitation sequence

# 1. Introduction

The 7xxx series aluminum alloys, or Al-Zn-Mg alloys, are widely recognized for their high strength-to-weight ratio and ability to undergo age hardening. Their mechanical properties, such as hardness, can be enhanced by forming fine precipitates during the aging heat treatment [1] to improve their mechanical properties by controlling the microstructure. Alloys with different Zn/Mg ratios exhibit distinct precipitate phases. Alloys with higher Zn and Mg content show improved mechanical properties due to a higher density of precipitates per unit area [2]. During aging, the G. P. zone forms at room temperature, and it is believed that the metastable  $\eta'$  phase forms directly from the solid solution at temperatures around 100-120°C, and transforms into the stable  $\eta$  phase (MgZn<sub>2</sub>) [3,4]. The  $\eta'$  phase, which has a plate-like morphology and hexagonal structure, is considered the main strengthening precipitate in Al-Zn-Mg(-Cu) alloys with a high Zn/Mg ratio [3]. The  $\eta$  phase, with a polytype [5] of Laves phases, has at least 15 different types, depending on their orientation with the aluminum matrix, as well as differences in morphology and size [6]. Among these,  $\eta_1$ ,  $\eta_2$ , and  $\eta_4$  are mostly observed precipitates in overaged Al-Zn-Mg alloys [7]. Allen and Vander [8] noted that the  $\eta_4$  phase is the most common crystallographic variant of  $\eta$  phases, forming heterogeneously along dislocations. In contrast, the metastable T' phase (Mg<sub>3</sub>Zn<sub>3</sub>Al<sub>2</sub> or Mg<sub>32</sub>(AlZn)<sub>49</sub>) is more common in alloys with a lower Zn/Mg ratio [3]. The T' phase rarely contributes to strength in these alloys and generally forms at high aging temperatures (above 200 °C) or in severely overaged conditions [9]. The calculated SAED (Selected Area Electron Diffraction) pattern for the (110)<sub>Al</sub> plane and the positions of the  $\eta/\eta'$  phase and T/T' phase were identified based on references from Zou et al. [10] and Zhang et al. [11] in Fig. 1 (a). Based on their morphology and characteristics, the precipitates in the Al-Zn-Mg alloy were classified and summarized in TABLE 1 [12-15].

Al-Zn-Mg with high Mg and aged at around 200°C were reported to be the condition that easy to form T/T' phase. Wang et al. [16] reviewed that the alloy composition has affected on the precipitation behavior of Al-Zn-Mg-Cu alloys. It suggests that increasing the Mg content can improve the volume fraction of precipitate phases during aging treatment, thereby enhancing yield strength. Yang et al. [17] reported an Al-Zn-Mg alloy strengthened by T phases, which exhibited excellent strength compared with alloy 7150 hardened by  $\eta$ -type phases. Zou et al. [18] reported that the clusters with different Zn/Mg ratios in Al-Zn-Mg-Cu showed different phase transformation path

Corresponding author: wanloliasanphiboon@gmail.com



UNIVERSITY OF TOYAMA, GRADUATE SCHOOL OF SCIENCE AND ENGINEERING, TOYAMA, JAPAN

UNIVERSITY OF TOYAMA, FACULTY OF SUSTAINABLE DESIGN, TOYAMA, JAPAN
 PROFESSOR EMERITUS, UNIVERSITY OF TOYAMA, TOYAMA, JAPAN

AISIN KEIKINZOKU CO., LTD, 12-3, TOYAMA, JAPAN

The precipitates found in the Al-Zı	1-Mg alloy
-------------------------------------	------------

Precipitates	Orientation relationship	Morphology (Habit plane)	Reference	
$\eta'$	$(0001)_{\eta'}//(1\overline{1}\overline{1})_{Al}; (10\overline{1}0)_{\eta'}//(110)_{Al}$	Plate on {111} <sub>Al</sub>	[12,13]	
$\eta_2$	$(0001)_{\eta'}//(1\overline{1}\overline{1})_{Al}; (10\overline{1}0)_{\eta'}//(110)_{Al}$	Plate on {111} <sub>Al</sub>	[12,13]	
$\eta_4$	$(11\overline{2}0_{\eta'}//(1\overline{1}\overline{1})_{Al}; [0001]_{\eta}//[110]_{Al}$	Rod/lath on {111} <sub>Al</sub>	[12,13]	
T'(T)	$(100)T//(111)_{Al}; (010)T//(112)_{Al}$	Globular, Cubic	[12-15]	

and co-precipitation of  $\eta'$  and T' phase enhances the strengthen of the alloy. However, there are still limited research about the precipitation sequence which occurs in this codition.

In this study, Al-Zn-Mg alloys with total Zn and Mg content around 8 at.% and a Zn/Mg ratio of 0.5 were investigated. The alloys were also refined with Ti and Zr. The aim was to understand how the high total at% of Zn and Mg, low Zn/Mg ratio and grain refiners affect age hardening and the microstructure, particularly at an aging temperature of around 200°C. Transmission electron microscopy (TEM) was used to observe the evolution of the microstructure, from the as-quenched state through various stages of aging.

# 2. Experimental procedure

An alloy labeled ZM35TZ, Z, M, T, and Z represents zinc (Zn), magnesium (Mg), titanium (Ti), and zirconium (Zr), respectively. Numbers 3 and 5 are the atomic percentages of Zn and Mg, respectively. The detailed composition of the investigated alloy is shown in TABLE 2, and a phase diagram was created by Thermo-Calc 2024a as Fig. 1(b) as a reference for the equilibrium state in the thermomechanical process.

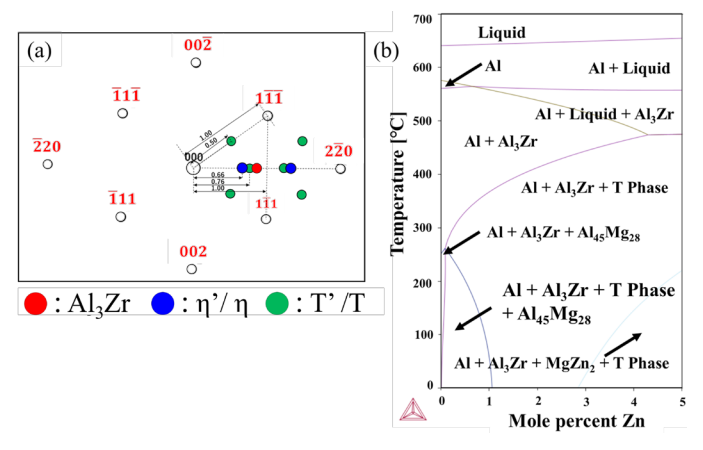


Fig. 1. (a) The stimulation of diffraction pattern of Al-Zn-Mg-Ti-Zr on taken from <110>Al (b) Phase diagram for ZM35TZ created by Thermo-Calc 2024a

This alloy was cast using a permanent steel mold, and the ingots were homogenized at 450°C for 24 hours. According to the phase diagram in Fig. 1(b), the Al matrix with no precipitates in this condition. Sheets of 1.5 mm thickness and 15 mm width were extruded, followed by cold rolling into 1.0 mm thick sheets.

TABLE 2 ZM35TZ Chemical Composition

ZM35TZ	Element					
	Zn	Mg	Ti	Zr	Al	Zn/Mg
at.%	2.79	5.61	0.01	0.01	Balance	0.50
wt.%	6.53	4.88	0.02	0.17	Balance	0.75

The sheets were solution heat treated at 475°C for 60 minutes in an air furnace and quenched into iced water. 4 conditions of hardness were as-quench and achieved by aging the material at 200°C in a silicone oil bath for 8 minutes, 64 minutes, and 2,000 minutes. At 200°C, the T phase can form in the Al matrix as the stable phase. The as-quenched condition sheet measured grain size using a Hitachi S-3500H scanning electron microscope (SEM) equipped with Nordlys HKL Technology EBSD detector. Micro Vickers hardness measurements were conducted using a Mitutoyo HM-101, with a 100 g (0.98 N) load and a holding time of 15 seconds. For TEM observation, the samples prepared as disks with a diameter of 3 mm were punched out from asquenched and aged foils, which were thinned to around 35 µm through mechanical and electrolytic polishing in a solution of 1/9 perchloric acid and 8/9 ethanol. These disks were further thinned to perforation using twin-jet electrolytic polishing on a Tenupol 3, in a solution of 1/3 nitric acid and 2/3 methanol, maintained between -30°C and -25°C. TEM observations were conducted using a Topcon EM-002B microscope at an acceleration voltage of 120 kV.

# 3. Results and Discussions

### 3.1. Micro Vickers hardness

The Micro Vickers hardness results are shown in Fig. 2(a). The Micro Vickers hardness (HV) was measured over an extended aging period. As the aging process continued at 200°C, from 2 minutes up to 100,000 minutes, the hardness initially measured around 90 HV in the as-quenched condition. In this condition, the microstructure can also be observed with SEM-EBSD with backscattered electrons as shown in Fig. 2(b). The crystal grain is fine with an avearage grain size of around 10.4  $\mu$ m  $\pm$  4 along the hot extrusion way. It increased to a peak hardness of approximately 120 HV, followed by a gradual decline, reaching around 90 HV at approximately 40,000 minutes, and continuing to decrease afterward.

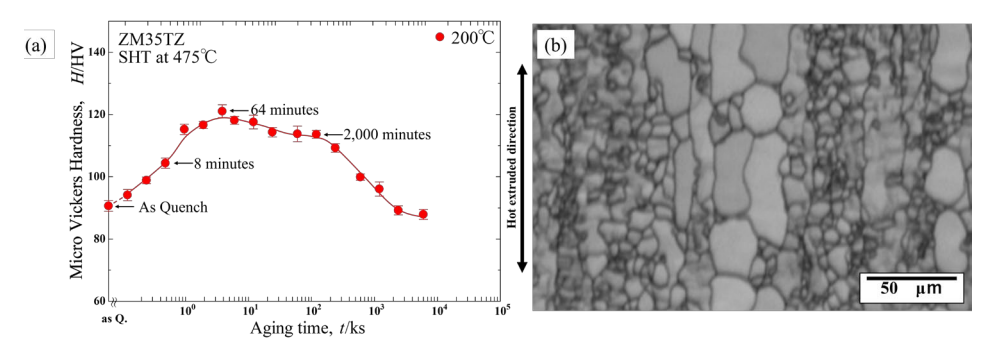


Fig. 2. (a) Age-hardening curves of ZM35TZ aged at 200°C (b) Backscattered electron image at the central area of ZM35TZ

# 3.2. TEM observation

According to the Micro Vickers hardness results, four conditions were selected for the TEM observation to examine the transformation of the microstructures: as-quenched, before peak aging (approximately 8 minutes), at peak aging (approximately 64 minutes) and, during overaging (approximately 2,000 min-

utes). Fig. 3(a) shows the SAED pattern at 64 minutes or peak aging and Fig. 3(b) zooms in the white rectangle with spots of precipitates, including the  $\eta'$ , T',  $\eta$ , and T phases, which became stronger and well-defined than as-quenched and aging at 8 minutes which is shown in Fig. 4(a-b) and Fig. 4 (d-e). In Fig. 3(c), based on the morphology in TABLE 1,  $\eta'$ ,  $\eta_2$ ,  $\eta_4$  and T'/T phases were defined in the bright-field image. Morphologies of the  $\eta'$ 

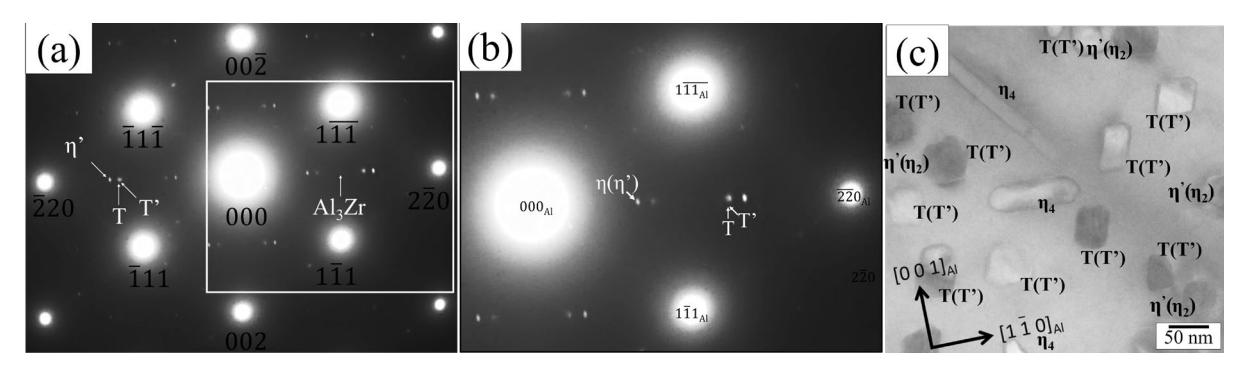


Fig. 3. (a-b) SAED pattern of Al-Zn-Mg-Ti-Zr taken from <110>Al (c) The corresponded bright-field images in peak aging condition

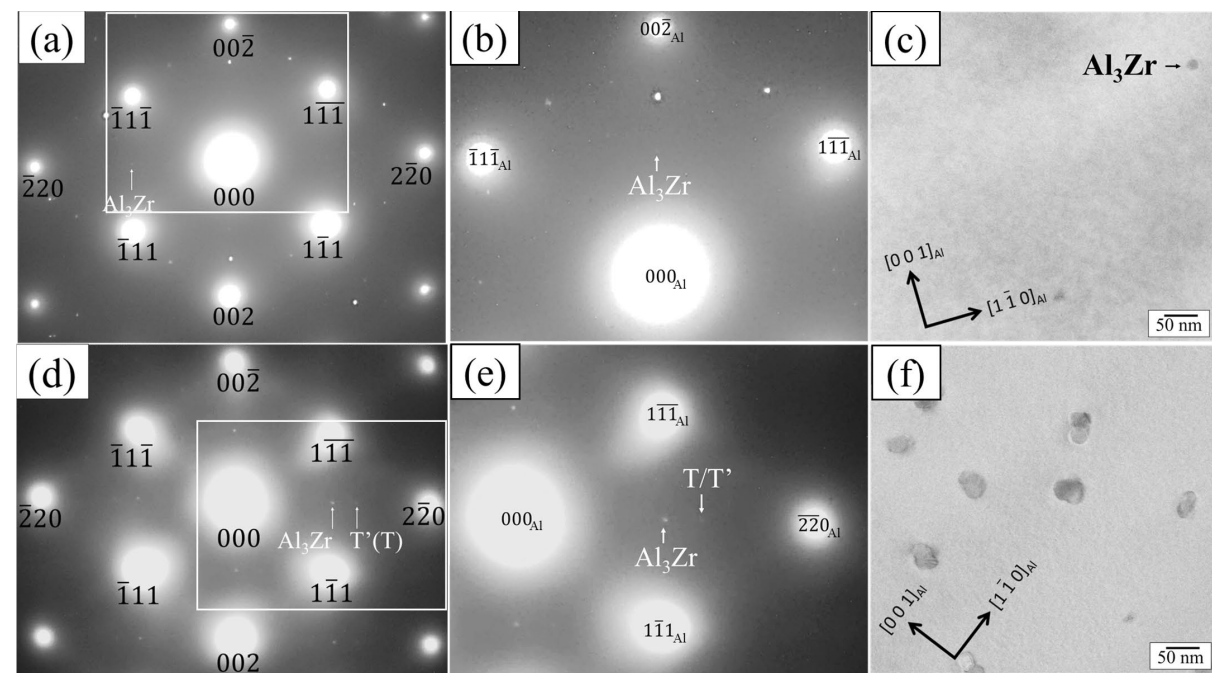


Fig. 4. (a-b and d-e) SAED pattern of Al-Zn-Mg-Ti-Zr taken from <110>Al (c and f) The corresponded bright-field images in as quench condition and aged at 8 minutes condition respectively

or  $\eta_2$  phase which is plate-like hexagonal shapes are observed.  $\eta_4$  phases which had a rod shape are long and large. High Zn content alloys in peak-aged conditions exhibit a higher density of T' phases and a smaller proportion of plate-like  $\eta'$  phases [19]. The main precipitate in this condition with a high number density is the T'/T phase. T'/T phases which are cubic and rectangular are observed. Both  $\eta'/\eta$  and T'/T phases were co-existed. This co-precipitation leads to optimal hardness [17].

In the as-quenched condition (observed within 6 hours after quenching), the diffraction of  $Al_3Zr$  dispersoids appeared bright and prominent, as shown in Fig. 4(a), and zoom in the white rectangle as shown in Fig. 4(b). The bright field image in Fig. 4(c) reveals  $Al_3Zr$  dispersoids and some small clusters and precipitates. After 8 minutes of aging, there were faint diffraction spots of the T'/T phase starting to emerge in Fig. 4(d) and zoomed in the white rectangle as shown in Fig. 4(e). In the Fig. 4(f), the precipitates were still smaller than precipitates in the peak aging, taking on cubic, and rectangular shapes assumed to be T'/T phases while the precipitates grew larger in rod and plate-liked shapes assumed to be  $\eta'/\eta$  phase. However, in this condition, we couldn't differentiate between the  $\eta'/\eta$  phases, and T'/T phases since all sizes and shapes were quite similar.

By the over-aging condition at 2,000 minutes, most known precipitate spots remained bright which were defined as  $\eta'/\eta$  phases, and T'/T phases (Fig. 5(a) and zoom in the white rectangle as shown in Fig. 5(b)). The T'/T phases' spots are stronger than  $\eta'/\eta$  phases' spots. This can mean the density of T'/T phases is higher than  $\eta'/\eta$  phases. However, in the bright field images (Fig. 5(c-d)) was observed that the number density of the  $\eta'/\eta$  phases is higher than the number density of T'/T phases. Fig. 5(c) and zoom in the white rectangle as shown in Fig. 5(d),

these bright field images show that  $\eta$  phase and T phase became significantly larger than the peak-aging condition. Compared to peak aging condition, defined  $\eta'$ ,  $\eta_2$ ,  $\eta_4$  and T'/T phases were still observed but other undefined  $\eta$  phases were observed.

Fig. 6(a) shows the relationship between the number density and the aging time. As the aging time increased, the number density, and size of precipitates grew, as shown in Fig. 6(a). The number density in percentage which calculated as 100% at the peak aging condition. The number density of clusters increased steadily from the as-quenched condition and decreased after peak aging. The number density of T'/T phases also increased and decreased after peak aging which can assume to continue in over aging. On the other hand, the number density of  $\eta'/\eta$  phases increased and stayed constant after the peak aging. Fig. 6(b) shows that the size of the  $\eta'/\eta$  and T'/T phases increased until peak aging. Both types of precipitates are quite similar. However, in the over-aging condition, the size of the  $\eta'/\eta$  phases increased significantly, while the T'/T phase grew more slowly. Since the hardness of the alloy decreased in over-aging with the larger size of the precipitates, especially the size of  $\eta$  phases that suddenly increased while the size of T phases constantly increased. Based on the phase diagram in Fig. 1(b), the equilibrium condition is supposed to be the T phase. However, according to our observation, it can be assumed that  $\eta$  phases expand, while some T phases dissolve back into the matrix, with some atoms integrating into other phases such as  $\eta_4$  that become longer and larger during overaging condition.

The precipitation sequence focusing on <110><sub>Al</sub> observed in this study is summarized in the schematic in Fig. 7. After solution heat treatment and quenching, no precipitates are visible but G. P. zones are likely to form as precursors for age-hardening

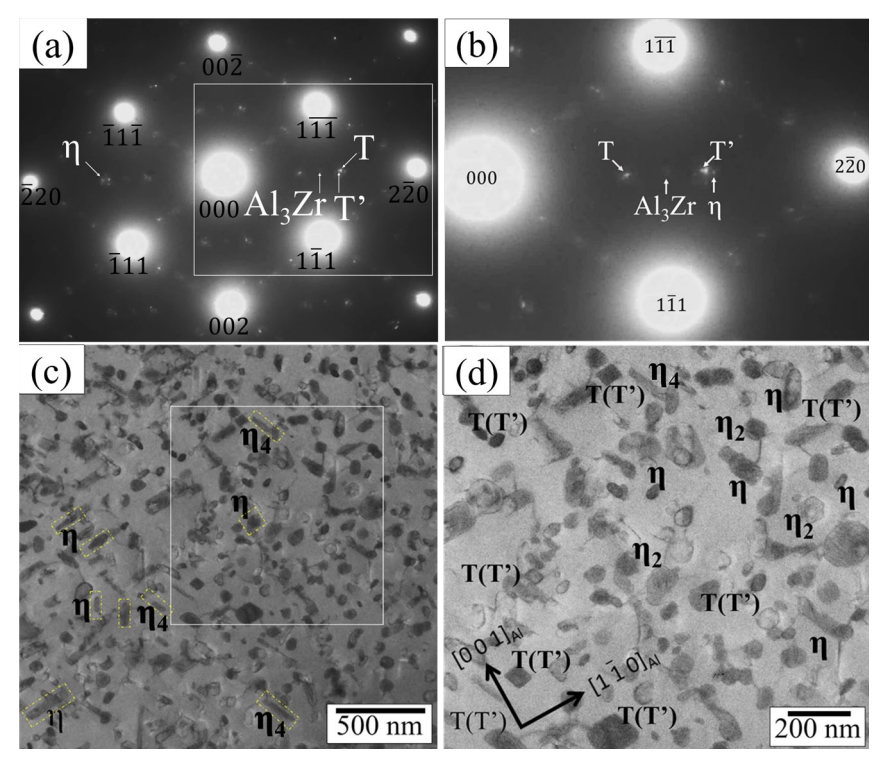


Fig. 5. (a-b) SAED pattern of Al-Zn-Mg-Ti-Zr taken from <110>Al (c-d) The corresponded bright-field images in over aging condition

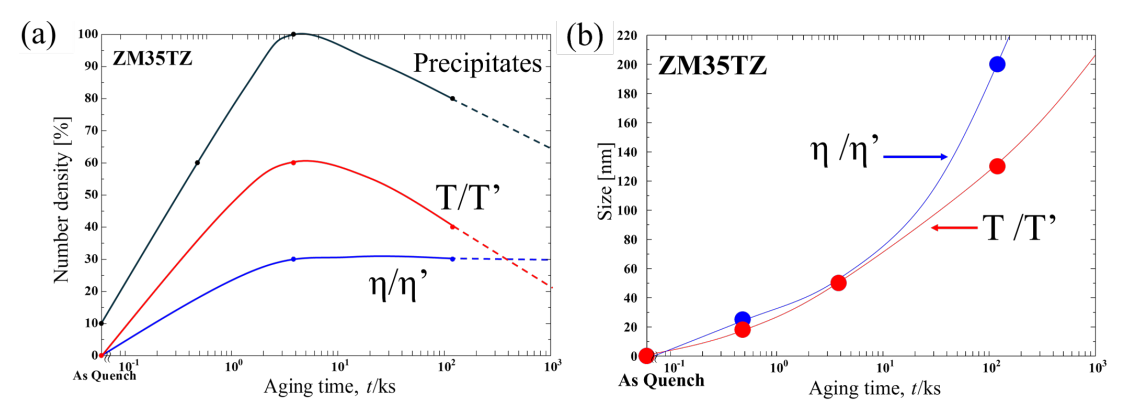


Fig. 6. (a) The relationship between the number density of precipitates and aging time (b) The relationship between size of  $\eta/\eta'$  and T/T' phases and aging time

phases such as the  $\eta'$  and T' phases, even though they were not directly observed (Fig. 7(a)). With the start of artificial aging, by 8 minutes (Fig. 7(b)), G. P. zones and small precipitates are present. These precipitates can be metastable phases ( $\eta'$  and T' phase) and stable phases ( $\eta$  and T phase). At 64 minutes (Fig. 7(c)), which corresponds to peak aging, G. P. zones transform into precipitates  $(\eta', T', \eta \text{ and } T \text{ phase})$ , primarily T' and T phases. Finally, in the over-aged condition (Fig. 7(d)), the precipitates grow larger while their number density decreases. During the overaging, the needlelike precipitates become coarsen, increase the average size and over-aged alloys indirectly suggest that the matrix precipitates are dissolved [20]. Additionally, substitutions can alter the phase's stability and transformation pathways which can lead to the formation of precipitates with varying compositions [21]. Since the number density of the T phase decreases while the  $\eta$  phase's size becomes larger. T phases may dissolve into the matrix and some atoms combine with the former  $\eta$  phase. Therefore, the  $\eta$ phase may change from MgZn<sub>2</sub> to Al-Zn-Mg precipitates due to the combination of dissolved T phase. Otherwise, the size of  $\eta$  phase become larger by the former atoms inside the matrix.

### 4. Conclusions

In this study, due to the low Zn/Mg ratio of this alloy and its aging at a high temperature (around 200°C), the precipitation behavior was analyzed. The main precipitates observed are the T' and T phases, which start to appear after 8 minutes of aging. At peak aging, T' and T phases take on distinct cubic and rectangular shapes. As aging progresses, the precipitates continuously increase in size and become more rounded. The  $\eta/\eta'$ phases, particularly  $\eta_4$  phases with rod-shaped precipitates are prominently observed during peak aging. In this stage,  $\eta_4$  phases elongated and grew longitudinally, resulting in sharper and more defined structures. At peak-aging hardness, the coexisting metastable phases ( $\eta'$  and T') contribute significantly to strengthening by impeding dislocation motion and achieving the peak-aging hardness. The size of the precipitates likely plays a key role in reaching optimal hardness, with specific types and sizes of precipitates contributing to the hardness. In the over-aging stage, the precipitates grew excessively large. The  $\eta$  phases expanded while the T phases may dissolve into the matrix or combined

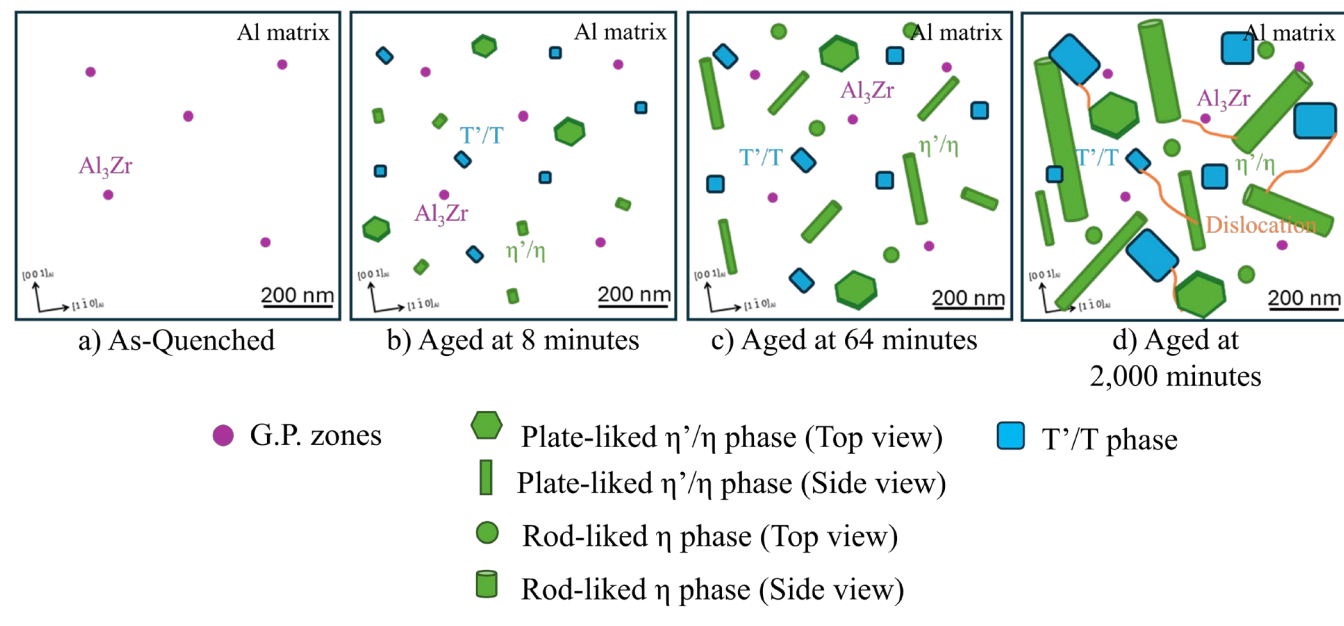


Fig. 7. Schematic of ZM35TZ precipitation sequence aged at 200°C from as-quenched to 2,000 minutes

with the former phases such as  $\eta$  phases leading to a decreased number density of precipitates. The former  $\eta$  phase may change from MgZn<sub>2</sub> to Al-Zn-Mg precipitates due to the incorporation of elements from the dissovled T phase during over-aging.

### Acknowledgment

This work was supported by AISIN KEIKINZOKU Co., LTD in providing the necessary materials for this research. Their commitment to advancing scientific inquiry is deeply appreciated. The results were presented during 14th Polish Japanese Joint Seminar on Micro and Nano Analysis (3-6.09.2024, Toyama, Japan

#### REFERENCE

- [1] E.A. Starke Jr., J.T. Staley, Application of modern aluminum alloys to aircraft. Progress in Aerospace Sciences 32, 131-172 (1996).
   DOI: https://doi.org/10.1016/0376-0421(95)00004-6
- [2] S. Lee, K. Watanabe, K. Matsuda, K. Nishimura, N. Numomura, H.Toda, K. Hirayama, K. Shimizu, H. Gao, M. Yamaguchi, K. Ebihara, M. Itakura, T. Tsuru, T. Yoshida, S. Murakami, S. Ikeno. Precipitation structure and mechanical properties on peak-aged Al-Zn-Mg alloys including different Zn/Mg ratios. Journal of Japan Institute of Light Metals 67 (5), 162-167 (2017). DOI: https://doi.org/10.2464/jilm.67.162
- [3] Y. Zou, X. Wu, S. Tang, Q. Zhu, H. Song, M. Guo, L. Cao. Investigation of microstructure and mechanical properties of Al-Zn-Mg-Cu alloys with various Zn/Mg ratios. Journal of Materials Science & Technology 85, 106-117 (2021). DOI:https://doi.org/10.1016/j.jmst.2020.12.045
- [4] A. Deschamps, Y. J. A. M. Brechet, Influence of deformation and aging of an Al–Zn–Mg alloy – II. Modeling of precipitation kinetics and yield stress. Acta Materialia 47 (1), 293-305 (1998). DOI: https://doi.org/10.1016/S1359-6454(98)00296-1
- [5] A. Bendo, T. Maeda, K. Matsuda, A. Lervik, R. Holmestad, C.D. Marioara, K. Nishimura, N. Nunomura, H. Toda, M. Yamaguchi, K. Ikeda, T. Homma, Characterisation of structural similarities of precipitates in Mg–Zn and Al–Zn–Mg alloys systems. Philosophical Magazine 99, 2619-2635 (2019). DOI: https://doi.org/10.1080/14786435.2019.1637032
- [6] H. Kim, H. Choi, J. Oh, S. Lee, H. Kwon, E. Park, S. Lee, G. Lee, M. Kim, H. Nam Han. Elucidating the role of a unique step-like interfacial structure of η<sub>4</sub> precipitates in Al-Zn-Mg alloy. Science Advances 9 (22), eadf7426 (2023).
  DOI: https://doi.org/10.1126/sciadv.adf742
- Y. Komura, K. Tokunaga. Structural studies of stacking variants in Mg-base Friauf–Laves phases. Acta Crystallographica Section
   B: Structural Crystallography and Crystal Chemistry 36 (7), 1548-1554 (1980). DOI: <a href="https://doi.org/10.1107/S0567740880006565">https://doi.org/10.1107/S0567740880006565</a>
- [8] R.M. Allen, J.B. Vander Sande, The oriented growth of precipitates on dislocations in Al-Zn-Mg – part I. Experimental observations. Acta Metallurgica 28 (9), 1185-1195 (1980). DOI: https://doi.org/10.1016/0001-6160(80)90073-5

- [9] N. Takata, M. Ishihara, A. Suzuki, M. Kobashi, Microstructure and strength of a novel heat-resistant aluminum alloy strengthened by T-Al6Mg11Zn11 phase at elevated temperatures. Materials Science and Engineering: A 739, 62-70 (2019). DOI: https://doi.org/10.1016/j.msea.2018.10.034
- [10] Y. Zou, X. Wu, S.Tang, Y. Wang, K. Zhao, L. Cao. The effect of pre-ageing/stretching on the ageing-hardening behavior of Al–Zn–Mg–Cu alloys correlated with Zn/Mg ratio. Materials Science and Engineering: A 830, 142331 (2022). DOI: https://doi.org/10.1016/j.msea.2021.142331
- [11] M. Zhang, C. Li, Y. Zhang, S. Liu, J. Jiang, J. Tang, L.Ye, X. Zhang. Effect of hot deformation on microstructure and quenchinginduced precipitation behavior of Al-Zn-Mg-Cu alloy. Materials Characterization 172, 110861 (2021). DOI: https://doi.org/10.1016/j.matchar.2020.110861
- [12] A. Bendo, K. Matsuda, A. Lervik, T. Tsuru, K. Nishimura, N. Nunomura, R. Holmestad, An unreported precipitate orientation relationship in Al-Zn-Mg based alloys. Materials Characterization 158, (2019). DOI: https://doi.org/10.1016/j.matchar.2019.109958
- [13] S.K Maloney, K. Hono, I.J Polmear, S.P Ringer, The effects of a trace addition of silver upon elevated temperature ageing of an Al–Zn–Mg alloy. Micron. 32 (8), 741-747 (2001). DOI: https://doi.org/10.1016/S0968-4328(00)00081-0
- [14] J. Chen, L. Zhen, S. Yang, W. Shao, S. Dai, Investigation of precipitation behavior and related hardening in AA 7055 aluminum alloy. Materials Science and Engineering: A 500, no. 1-2, 34-42 (2009). DOI: https://doi.org/10.1016/j.msea.2008.09.065
- [15] G. Bergman, J. L. Waugh, L. Pauling, The crystal structure of the metallic phase Mg32 (Al, Zn) 49. Acta Crystallographica 10 (4), 254-259 (1957).
   DOI: https://doi.org/10.1107/S0365110X57000808
- [16] J. Wang, F. Li, Research Status and Prospective Properties of the Al-Zn-Mg-Cu Series Aluminum Alloys. Metals 13 (8), (2023). DOI: https://doi.org/10.3390/met13081329
- [17] X.B. Yang, J.H. Chen, J.Z. Liu, F. Qin, J. Xie, C.L. Wu, A high-strength AlZnMg alloy hardened by the T-phase precipitates. Journal of Alloys and Compounds 610, (2014). DOI: https://doi.org/10.1016/j.jallcom.2014.04.185
- [18] Y. Zou, X. Wu, S. Tang, Q. Zhu, H. Song, L. Cao, Co-precipitation of T' and η' phase in Al-Zn-Mg-Cu alloys. Materials Characterization 169, 110610 (2020). DOI: https://doi.org/10.1016/j.matchar.2020.110610
- [19] A. Ahmed, S. Lee, T. Tsuchiya, K. Matsuda, K. Nishimura, N. Numomura, H. Toda, K. Hirayama, K. Shimizu, M. Yamaguchi, T. Tsuru, Microstructure observation of T-phases in Al-Zn-Mg alloy with low Zn/Mg ratio. SSRN. DOI: http://dx.doi.org/10.2139/ssrn.4900094
- [20] L. Liu, Y. Hou, T. Ye, L. Zhang, X. Huang, Y. Gong, C. Liu, Y. Wu, S. Duan, Effects of Aging Treatments on the Age Hardening Behavior and Microstructures in an Al-Mg-Si-Cu Alloy. Metals 14 (2), 238 (2024). DOI: https://doi.org/10.3390/met14020238
- [21] M.J. Styles, T.J. Bastowm, M.A. Gibson, C.R. Hutchinson, Substitution of Cu and/or Al in  $\eta$  phase (MgZn<sub>2</sub>) and the implications for precipitation in Al-Zn-Mg-Cu alloys. Intermetallics **49**, 40-51 (2014). DOI: http://dx.doi.org/10.1016/j.intermet.2014.01.012